4316

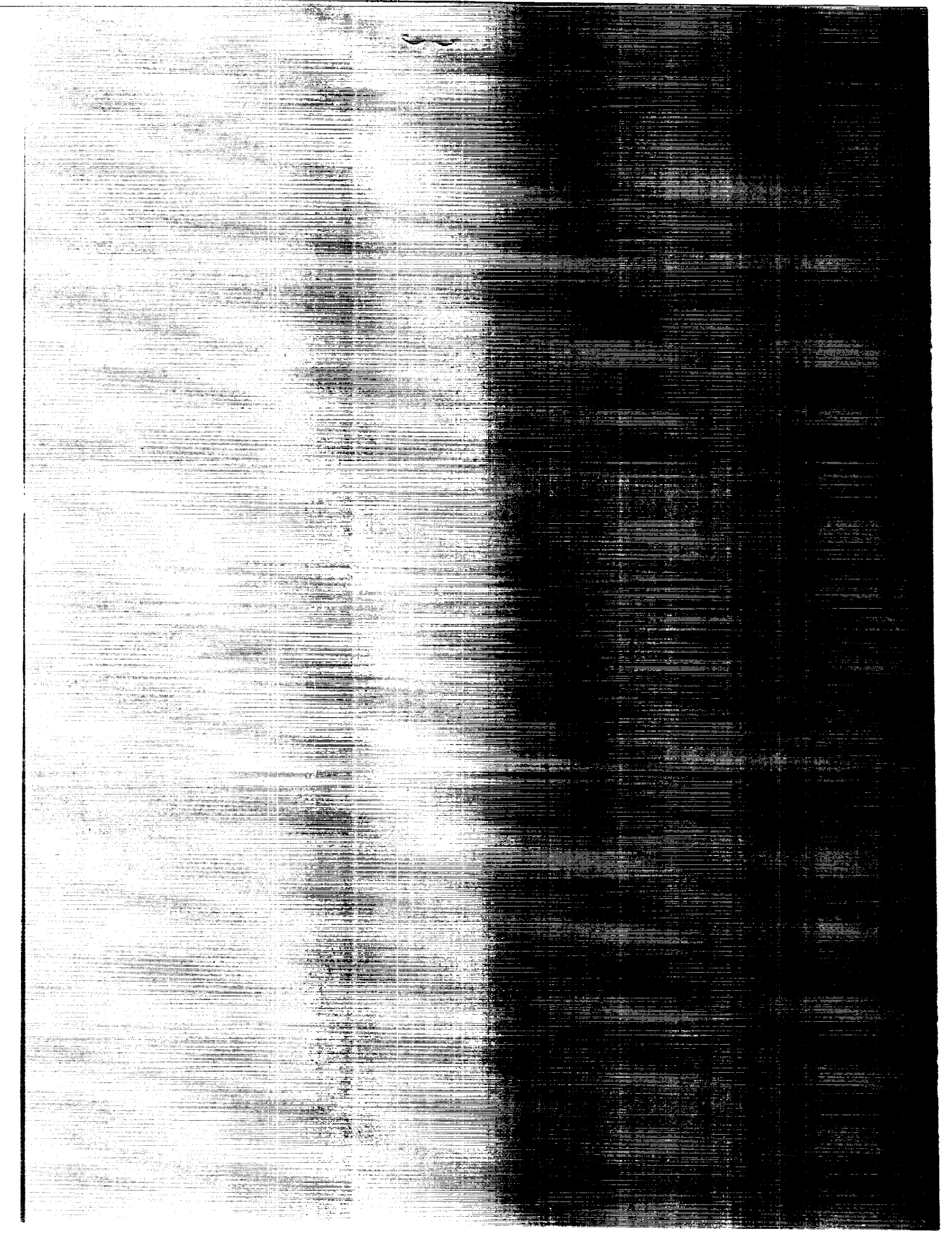

NASA Technical Memorandum 4316

Effect of Solidity and Inclination on Propeller-Nacelle Force Coefficients

Garl L. Gentry, Jr., and Dana Morris Dunham
Langley Research Center
Hampton, Virginia

M. A. Takallu
Lockheed Engineering & Sciences Company
Hampton, Virginia

National Aeronautics and
Space Administration

Office of Management

Scientific and Technical
Information Program

1991

Abstract

A series of wind tunnel experiments was conducted to study the effect of propeller solidity and thrust axis inclination on the propeller normal-force coefficient. Experiments were conducted in the Langley 14- by 22-Foot Subsonic Tunnel with a sting-mounted, counterrotation, scale-model propeller and nacelle. Configurations had two rows of blades with combinations of 4 and 8 blades per hub. The solidity was varied by changing the number of blades on both rows. Tests were conducted for blade pitch settings of 31.34°, 36.34°, *and* 41.34° *over a range of angle of attack from* −10° *to* 90° *and a range of advance ratio from 0.8 to 1.4. The increase in propeller normal force with angle of attack is greater for propellers with higher solidity.*

Introduction

Although decades of experience exist for propeller driven aircraft, this experience has been for configurations having significantly lower power loadings than those presently being considered. Investigations (refs. 1 through 4) indicated that wing- and aft-fuselage-mounted advanced turboprop configurations appear feasible and that configuration selection depends on further information regarding acoustic treatment requirements, structural weight, and engine-airframe installation aerodynamics. This research indicates that one impact of the high disk loading associated with advanced turboprop installations is increased aircraft stability during operations which expose the propeller to high inflow angles in either pitch or yaw. Such operations include the take-off, climb, and approach phases of flight and ground operations in crosswinds. These increases in stability are not always beneficial since they may require higher levels of control to maneuver the aircraft.

The problem of an inclined propeller is one of many installation problems that are related to the nonuniformity of the flow past the blades. A nonuniform inflow can alter vibrational and aeroacoustic behavior of the operating propeller. Other examples of these problems are counterrotating propellers where the aft blade row is exposed to a highly nonuniform wake produced by the upstream blade row and pusher configurations where the blades are exposed to the wake of the upstream wing-pylon. For the pusher configurations, because of the asymmetrical variation of the blade section angle of attack, the loads experienced by the blades are cyclic (ref. 5), and thus the propeller blades experience time-dependent forces and moments. These cyclic loads (ref. 6) may cause additional noise (ref. 7) or vibrational problems (ref. 8). In the present report, the focus is on the nonuniformity of the inflow caused by the propeller inclination.

The investigation discussed herein is part of a broad NASA research program to obtain fundamental aerodynamic information regarding advanced turboprop installation effects. Data from early research (ref. 9) on lightly loaded propellers showed a strong dependence of propeller normal force on blade solidity. Also, limited data on more highly loaded propellers (ref. 10) showed that a counterrotation propeller at thrust-axis (nacelle) angles of attack produced substantially higher values of normal force than did a single rotation propeller with the same solidity. The present investigation was conducted to extend the research to provide baseline information regarding the effect of changing the solidity by changing the number of blades on the force and moment characteristics of an isolated counterrotation turboprop-nacelle combination operating over a range of angle of attack from −10° to 90°, a range of advance ratio from 0.8 to 1.4, and at blade pitch angles of 31.34°, 36.34°, and 41.34°. Tests were conducted in the Langley 14- by 22-Foot Subsonic Tunnel (ref. 11).

Symbols

a_1	induced velocity fraction in axial direction
a_2	induced velocity fraction in circumferential direction
B	blade area, ft^2
C_N	normal-force coefficient, $\dfrac{\text{Normal force}}{qS}$
C_T	thrust coefficient, $\dfrac{\text{Thrust}}{\rho n^2 D^4}$
C_Y	side-force coefficient, $\dfrac{\text{Side force}}{qS}$
c	blade section chord, ft

c_n	sectional load in normal-force direction, $\frac{\text{Section normal force}}{\rho w^2 c/2}$
c_t	sectional load in thrust direction, $\frac{\text{Section thrust}}{\rho w^2 c/2}$
c_y	sectional load in side-force direction, $\frac{\text{Section side force}}{\rho w^2 c/2}$
D	propeller diameter, ft
J	propeller advance ratio, $\frac{V_\infty}{nD}$
N	number of blades
n	propeller rotational speed, rps
q	free-stream dynamic pressure, lb/ft^2
R	propeller radius, $\frac{D}{2}$, ft
r	distance along propeller radius, normalized by R
S	propeller disk area, ft^2
t	time, sec
V_∞	free-stream velocity, ft/sec
v_a	section axial inflow velocity, ft/sec
v_t	section rotational inflow velocity, ft/sec
w	section velocity, ft/sec
x	distance along X-axis, in.
α	section angle of attack, deg
α_p	propeller inclination (nacelle angle of attack), deg
β	blade pitch angle, deg
$\beta_{0.75}$	nominal blade angle at $0.75R$, deg
ρ	free-stream density, $slugs/ft^3$
σ	solidity, NB/S
ϕ	inflow angle, deg
ψ	azimuthal position
Ω	rotational frequency, rad/sec

Test Apparatus

Propellers

Photographs of the propeller-nacelle model used in this investigation are shown in figures 1 and 2. The single rotation propeller blade design, designated SR-2, used for the tests reported in reference 1 was used in counterrotation arrangement for this study and the one in reference 12. The detailed geometry of the SR-2 blade design is documented in reference 13. In order to simulate a representative ratio of propeller diameter to hub diameter with the single rotation blades of reference 13 in a counterrotation arrangement, the SR-2 blade coordinates were scaled to a diameter of 15 in. and then shifted radially to accommodate the hub requirements. This resulted in a hub diameter of 2.25 in. and a propeller diameter of 16.1 in. The reference chord in the original single rotation model (ref. 13) was located at the 0.75 radial station. For this model, this reference point was moved to the 0.79 radial station. To obtain the blade pitch angle at the 0.75 radial station of the current configuration, an increment of 1.34° was added to the 0.79 angle setting. The hubs allowed 0, 2, 4, or 8 blades on either or both blade rows. Blade angles were adjusted with a collective pitch-change gear which permitted a continuous range of blade angle setting with an accuracy of ±0.25°. The blade angle used in this investigation is the average angle of the blades at the 0.75 radial station. For these tests, both blade rows of the counterrotation system were set at the same pitch setting. The spacing between the pitch-change axis of the blade rows was 2.31 in. ($0.287R$). The front row of blades was driven counterclockwise looking upstream. The counterrotation gearbox consisted of two gears and two pinions which drove the rear blade row at the same speed but in the direction opposite to that of the front blade row.

Nacelle and Support System

The dimensional characteristics of the propeller-nacelle are given in tables 1 and 2 and are shown in figure 3. The nacelle used in this investigation was a body of revolution with maximum outside diameter of 6 in. and housed a water-cooled electric motor which was rated at 29 hp at 10 000 rpm. A fairing which covered the counterrotation gearbox smoothly transitioned from the hub diameter to the nacelle diameter. The nacelle was mounted as a straight extension of a straight sting.

Facility

Tests were conducted in the Langley 14- by 22-Foot Subsonic Tunnel, which has a test section 14.50 ft high by 21.75 ft wide. This is a closed-circuit atmospheric wind tunnel and is described in reference 11. The nacelle was mounted on a model

support cart shown in figure 4 which allowed the nacelle to be rotated to different angles of attack and sideslip while remaining at the tunnel centerline to minimize wall interference effects.

Test Conditions

Data were obtained at a free-stream dynamic pressure of 4.5 psf, which represents a tunnel speed of 63 fps. The free-stream velocity of 63 fps was chosen to give an advance ratio in the range from 0.8 to 0.9 for the 8- by 8-blade propeller at the maximum available power from the electric motor. The corresponding dynamic pressure of 4.5 psf was then used for all the propeller configurations. Propeller operating conditions were selected by first setting the tunnel dynamic pressure and then setting advance ratio using propeller rotational speed (rpm). These conditions were held constant throughout a given sweep of angle of attack or sideslip. Aerodynamic forces and moments were measured with a six-component strain-gauge balance located inside the nacelle with the balance moment center as indicated in figure 3. All data presented are time averaged and were acquired at a rate of 20 samples/sec for 5 sec.

Results and Discussion

The theoretical relations and definitions between the inclination angle α_p, solidity σ, and the time-averaged coefficients of thrust C_T, normal force C_N, and side force C_Y are briefly discussed in the appendix. The data are presented for the combined propeller-nacelle configuration in terms of the time-averaged coefficients. First, data are presented for the entire angle-of-attack range from $-10°$ to $90°$ for the 8- by 8- (8 blades in front row and 8 blades in second row) and 4- by 4-blade propellers for three different advance ratios to illustrate the variation of thrust and normal force due to the propeller inclination. Then, data are presented for selected angles of attack as a function of advance ratio for the 8- by 8-, 8- by 4-, and 4- by 4-blade propellers. Finally, data are presented as a function of solidity.

Figures 5 and 6 show the variation of thrust and normal-force coefficients as a function of propeller inclination α_p, for different values of propeller advance ratio. The data in figure 5 for the 8- by 8-blade configuration, which has a solidity of 0.56, indicate that, for a constant rotational speed, both thrust and normal-force coefficients increase in magnitude as α_p increases. Thrust coefficient remains nearly constant between $\alpha_p = -10°$ and $10°$ and then begins to increase as α_p increases, although the rate of increase is dependent on advance ratio. Normal-force coefficient is also dependent on advance ratio with C_N increasing more rapidly for decreasing advance ratio. In an examination of the data for all three advance ratios, the increase in C_N seems to be nearly linear over the range of α_p up to approximately $60°$ after which the rate of change begins to decrease. Similar trends are observed in figure 6 for the 4- by 4-blade configuration with solidity of 0.28. For the lower solidity, the linear range for C_N seems to be somewhat smaller. A comparison of the normal-force coefficients in figures 5(b) and 6(b) shows that at a constant advance ratio a higher maximum value for C_N is obtained for the propeller with higher solidity. Further analysis of the data is restricted to the linear range ($\alpha_p = 0°$ to $30°$).

Figures 7, 8, and 9 show the variation of C_Y, C_T, and C_N as a function of propeller advance ratio J, for various values of α_p for the 8- by 8- ($\sigma = 0.56$), the 8- by 4- ($\sigma = 0.42$), and the 4- by 4- ($\sigma = 0.28$) blade configurations, respectively. For all these configurations, at these blade angles the thrust coefficient decreases with increasing advance ratio (lower loading). This decrease in thrust coefficient has a steeper slope for the highest propeller solidity. The normal- and side-force coefficients are very small for $\alpha_p = 0°$. For all solidities, normal-force coefficient showed much more sensitivity than the other coefficients to changes in α_p and J, as would be expected.

Better insight into the sensitivity to solidity changes can be gained by presenting the force coefficients as a function of the advance ratio for different values of solidity on a single figure, as shown in figure 10 for $\alpha_p = 0°$ and $20°$. As expected, the normal-force coefficient remains small for all values of propeller solidity when $\alpha_p = 0°$. The increase in the level of C_N with higher solidity is evident in the data for $\alpha_p = 20°$.

Figure 11 illustrates the variation of C_Y, C_T, and C_N with respect to propeller solidity for various values of α_p. The blade pitch at the 0.75 radial station was $41.34°$ and the advance ratio was 1.1. As α_p increases, the level of normal force increases. Normal-force coefficient also increases with increasing solidity. The magnitude of this change is more pronounced at higher nacelle angles of attack. Although the side force for all angles of attack is expected to remain 0 for a counterrotation system, the data show nonzero side force. Thrust coefficient also increases with increasing solidity; however, its increase is not as pronounced with increasing nacelle angle of attack as that of the normal-force coefficient.

The results shown in figures 12 and 13 are for lower advance ratios, $J = 1.0$ and 0.9, respectively.

Although these cases represent higher loading than the case shown in figure 11, similar trends in the data may be seen. The increase in solidity and nacelle angle of attack results in an increase in the level of C_N. To illustrate the combined effects of solidity and advance ratio more clearly, the variation of C_N with respect to σ for the three different advance ratios at $\alpha = 20°$ is shown in figure 14. The higher loaded conditions result in a higher normal-force coefficient for a given solidity.

Summary of Results

A wind tunnel investigation has been conducted with a counterrotation propeller with SR-2 blades operated with 4 and 8 blades per hub to vary solidity. For a propeller with the thrust axis at an angle of attack, the results may be summarized as follows:

1. The normal force associated with nonzero angles of attack increases linearly at lower angles of attack but the rate of increase decreases after an angle of attack of 30°.

2. The level of normal force is higher for propellers with higher solidity and for higher thrust operating conditions.

3. Increasing the number of blades in the front row (from 4 by 4 to 8 by 4) is more effective at increasing thrust than increasing the number of blades in the back row (from 8 by 4 to 8 by 8).

NASA Langley Research Center
Hampton, VA 23665-5225
November 22, 1991

Appendix
Theoretical Relations and Definitions of Various Parameters

According to strip theory, for the propeller axis at an angle of attack of 0°, the section lift and drag forces remain constant with the blade azimuthal position. The section angle of attack is only influenced by the induced velocities due to helical velocity vector. However, the section lift and drag coefficients are dependent on the section angle of attack and the section velocity which are defined as

$$\alpha = \beta - \phi \tag{1}$$

and

$$w = \frac{v_q}{\cos\phi} \tag{2}$$

where β indicates the section pitch angle with respect to the plane of rotation. In equation (2), v_q and ϕ are the circumferential velocity and helical angle, respectively, and are defined below. As illustrated in figure 15, v_a is defined as the axial velocity and is assumed to vary from the free-stream velocity by a fraction of V_∞ as

$$v_a = V_\infty(1 + a_1) \tag{3}$$

In the same manner, v_q is defined as circumferential velocity and is assumed to differ from the rotational velocity $r\Omega$ by a fraction a_2 as

$$v_q = r\Omega(1 - a_2) \tag{4}$$

In equation (4), r is defined as the radial station along the blade and Ω is the propeller rotational speed. Finally, ϕ becomes

$$\phi = \tan^{-1}\frac{v_a}{v_q} \tag{5}$$

In reference 14, it is shown that induced velocity fractions a_1 and a_2 can be obtained from balancing the linear and angular momenta around the propeller and its wake. The resulting expressions found for a_1 and a_2 are related to the circulation distribution in the radial direction and propeller solidity σ where

$$\sigma = \frac{NB}{S} \tag{6}$$

The sectional lift and drag then define the thrust and torque coefficients, whereas normal and side forces vanish throughout the cycle due to symmetric loading.

Once the propeller axis is set at an inclination to the incoming flow, both axial and circumferential velocities v_a and v_q must be modified for the propeller inclination α_p as follows:

$$v_a = (1 + a_1)\, V_\infty \cos\alpha_p \tag{7}$$

$$v_q = (r\Omega + V_\infty \sin\alpha_p \cos\psi)\,(1 - a_2) \tag{8}$$

Consequently, the inflow angle ϕ and angle of attack α vary with azimuthal position ψ. This variation is illustrated in the sketches in figure 16. Sectional lift and drag become functions of azimuthal position and the thrust axis inclination. Thus, the sectional force coefficients in the plane of rotation such as sectional normal-force coefficient c_n and sectional side-force coefficient c_y become

$$c_t = f\,(\alpha_p, \psi, r\Omega, V_\infty, \sigma) \tag{9}$$

$$c_n = f\,(\alpha_p, \psi, r\Omega, V_\infty, \sigma) \tag{10}$$

$$c_y = f\,(\alpha_p, \psi, r\Omega, V_\infty, \sigma) \tag{11}$$

In theoretical calculations, the instantaneous propeller force coefficients are computed from the integration of distributed loads along each blade in the radial direction so that

$$C_T(t) = f\,(\alpha_p, J, \sigma) \tag{12}$$

$$C_N(t) = f\,(\alpha_p, J, \sigma) \tag{13}$$

$$C_Y(t) = f\,(\alpha_p, J, \sigma) \tag{14}$$

For 0° inclination, the time-averaged values of total normal and side forces should remain zero. For the propeller at some angle of attack, the time-averaged values of these forces are the mean value over a full propeller blade cycle and are

$$C_T = f\,(\alpha_p, J, \sigma) \tag{15}$$

$$C_N = f\,(\alpha_p, J, \sigma) \tag{16}$$

$$C_Y = f\,(\alpha_p, J, \sigma) \tag{17}$$

The expressions in equations (15) through (17) correspond to the experimental results presented in the main body of this report.

References

1. Applin, Zachary T.; and Coe, Paul L., Jr.: *Low-Speed Stability and Control Characteristics of a Transport Model With Aft-Fuselage-Mounted Advanced Turboprops.* NASA TP-2535, 1986.

2. Coe, Paul L., Jr.; Applin, Zachary T.; and Williams, Louis J.: Stability and Control Results for Advanced Turboprop Aft-Mount Installations. *SAE 1984 Transactions*, Volume 93, Soc. of Automotive Engineers, Inc., c.1985, pp. 6.256–6.263. (Available as SAE Paper 841479.)

3. Ridder, Sven-Olof: Wind Tunnel Test of a Twin, Rear Propeller Transport Aircraft Configuration at Low Speeds. *ICAS Proceedings 1984—14th Congress of the International Council of the Aeronautical Sciences*, Volume 2, B. Laschka and R. Staufenbiel, eds., International Council of Aeronautical Sciences, c.1984, pp. 644–654. (Available as ICAS-84-2.6.3.)

4. Aljabri, A. S.: Wind Tunnel Tests on a One-Foot Diameter SR-7L Propfan Model. AIAA-87-1892, June–July 1987.

5. Takallu, M. A.: *Unsteady Potential Flow Past a Propeller Blade Section.* NASA CR-4307, 1990.

6. Takallu, M. A.; and Spence, P. L.: Prediction of Unsteady Thrust and Torque Coefficients for a Pusher Propeller. AIAA-87-2630, Aug. 1987.

7. Takallu, M. A.; and Block, P. J. W.: Prediction of Added Noise Due to the Effect of Unsteady Flow on Pusher Propellers. AIAA-87-0255, Jan. 1987.

8. Martinez, Rudolph: *Predictions of Unsteady Wing and Pylon Forces Caused by Propeller Installation.* NASA CR-178298, 1987.

9. Ribner, Herbert S.: *Formulas for Propellers in Yaw and Charts of the Side-Force Derivative.* NACA Rep. 819, 1945. (Supersedes NACA ARR 3E19.)

10. Dunham, Dana Morris; Gentry, Garl L., Jr.; and Coe, Paul L., Jr.: *Low-Speed Wind-Tunnel Tests of Single- and Counter-Rotation Propellers.* NASA TM-87656, 1986.

11. Gentry, Garl L., Jr.; Quinto, P. Frank; Gatlin, Gregory M.; and Applin, Zachary T.: *The Langley 14- by 22-Foot Subsonic Tunnel: Description, Flow Characteristics, and Guide for Users.* NASA TP-3008, 1990.

12. Dunham, Dana Morris; and Gentry, Garl L., Jr.: The Effect of Solidity on Propeller Normal Force. *SAE 1989 Transactions—Journal of Aerospace*, Section 1—Volume 98, 1989, pp. 1232–1237. (Available as SAE Paper 892205.)

13. Jeracki, Robert J.; Mikkelson, Daniel C.; and Blaha, Bernard J.: *Wind Tunnel Performance of Four Energy Efficient Propellers Designed for Mach 0.8 Cruise.* NASA TM-79124, 1979. (Available as SAE Paper 790573.)

14. Takallu, M. A.; and Dunham, Dana Morris: A Hybrid Method for Prediction of Propeller Performance. AIAA-90-0440, Jan. 1990.

Table 1. Dimensional Characteristics

Counterrotation propeller diameter, in.	16.10
Spacing between blade row, in.	2.30
Hub diameter, in.	4.50
Maximum nacelle diameter, in.	6.00
Distance of moment reference center aft of forward propeller disk, in.	38.24

Table 2. Nacelle Coordinates

x, in.	r, in.	x, in.	r, in.
0.000	0.000	12.766	2.982
0.028	0.149	12.904	2.986
0.528	0.525	13.180	3.000
1.028	0.857		
1.528	1.140	34.028	3.000
2.028	1.405	36.028	2.940
2.528	1.638	37.028	2.900
3.028	1.845	38.028	2.850
3.528	2.015	39.028	2.520
4.028	2.145	40.028	2.300
4.528	2.235	41.028	2.160
4.778	2.250	42.028	2.020
		43.028	1.920
9.248	2.250	43.745	1.831
9.918	2.333	44.028	1.820
10.618	2.545	45.028	1.750
11.068	2.685	46.028	1.680
11.628	2.840	47.028	1.620
12.258	2.935	48.028	1.600
12.628	2.970	49.028	1.560
12.645	2.976	49.345	1.550

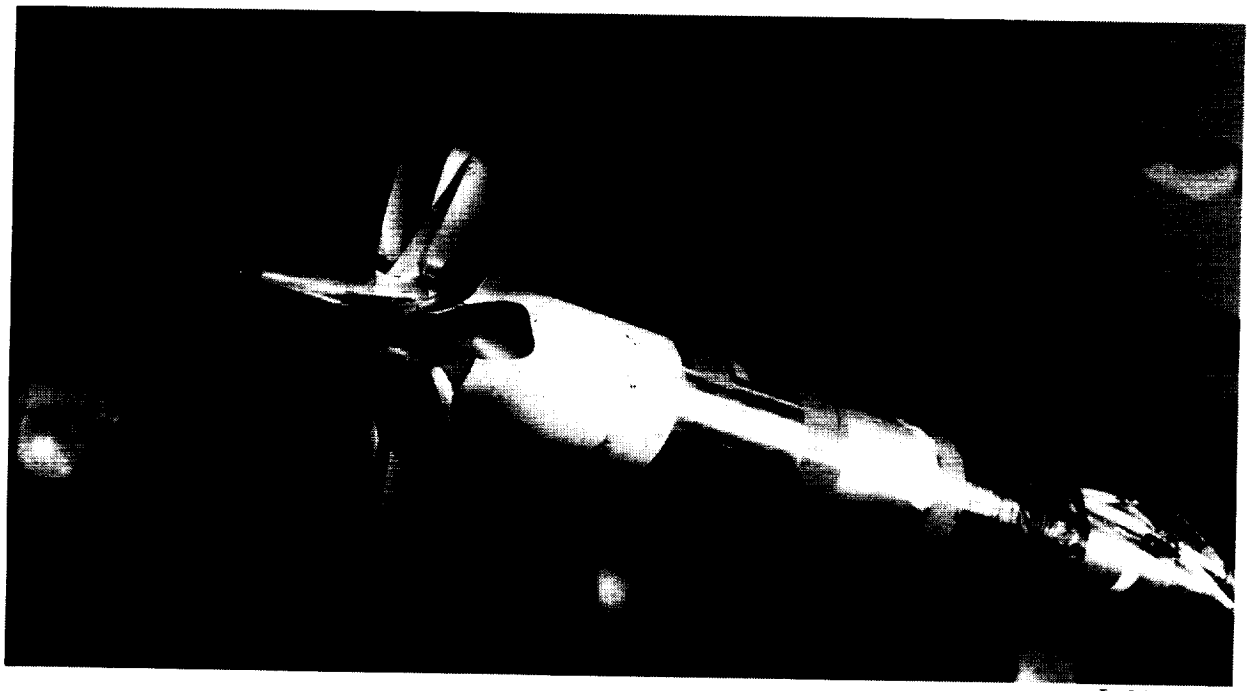

L-91-14546

Figure 1. Propeller-nacelle model mounted for tests.

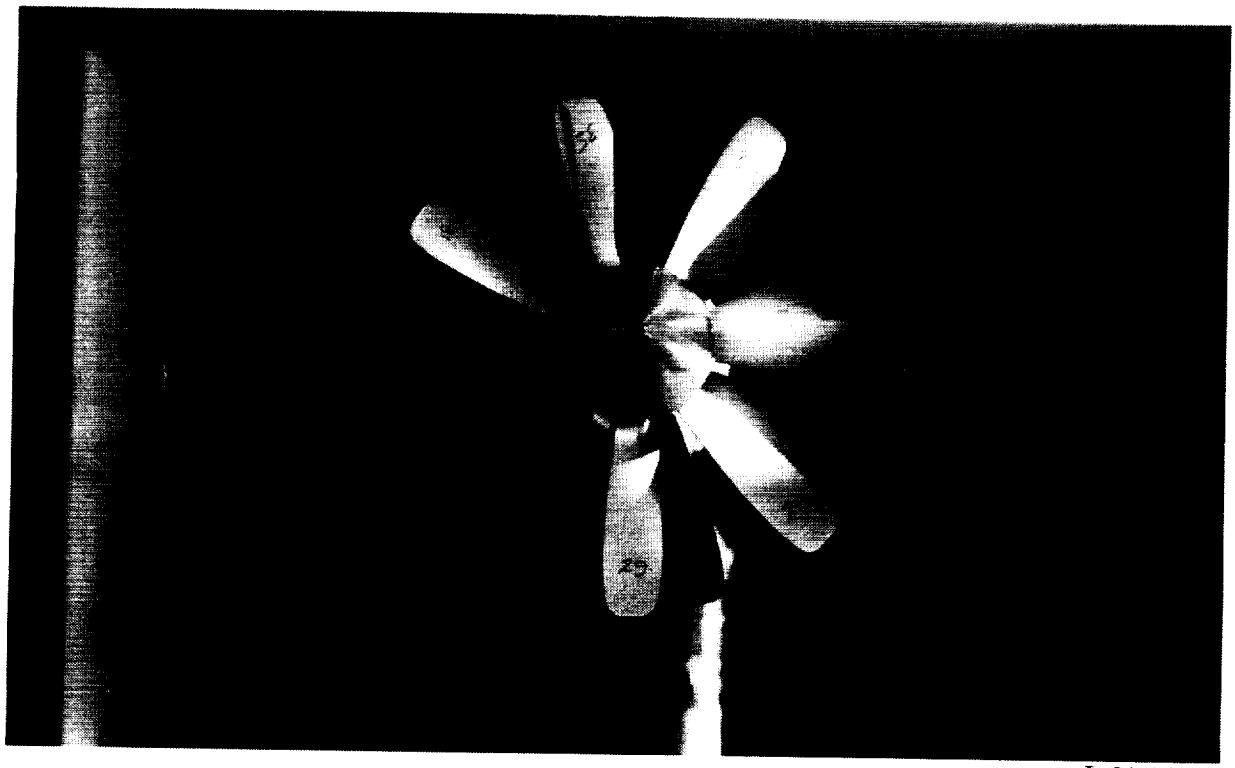

L-91-14547

Figure 2. Close-up of 8- by 8-blade propeller.

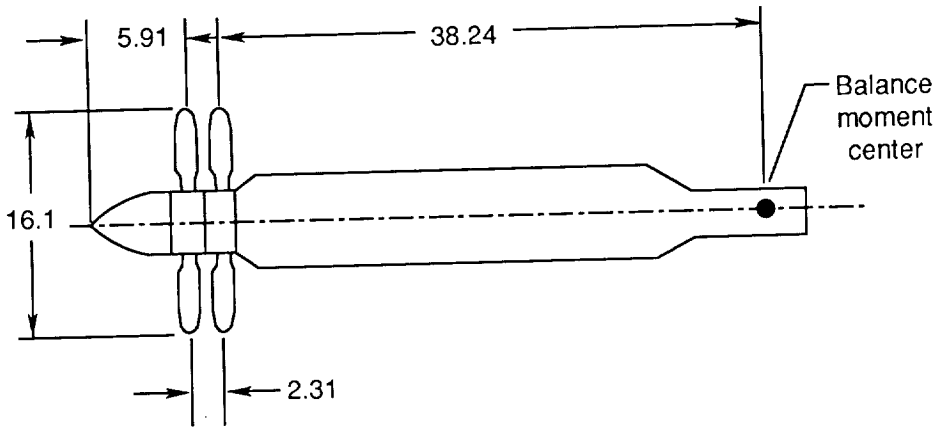

Figure 3. Sketch of propeller-nacelle model. Linear dimensions are in inches.

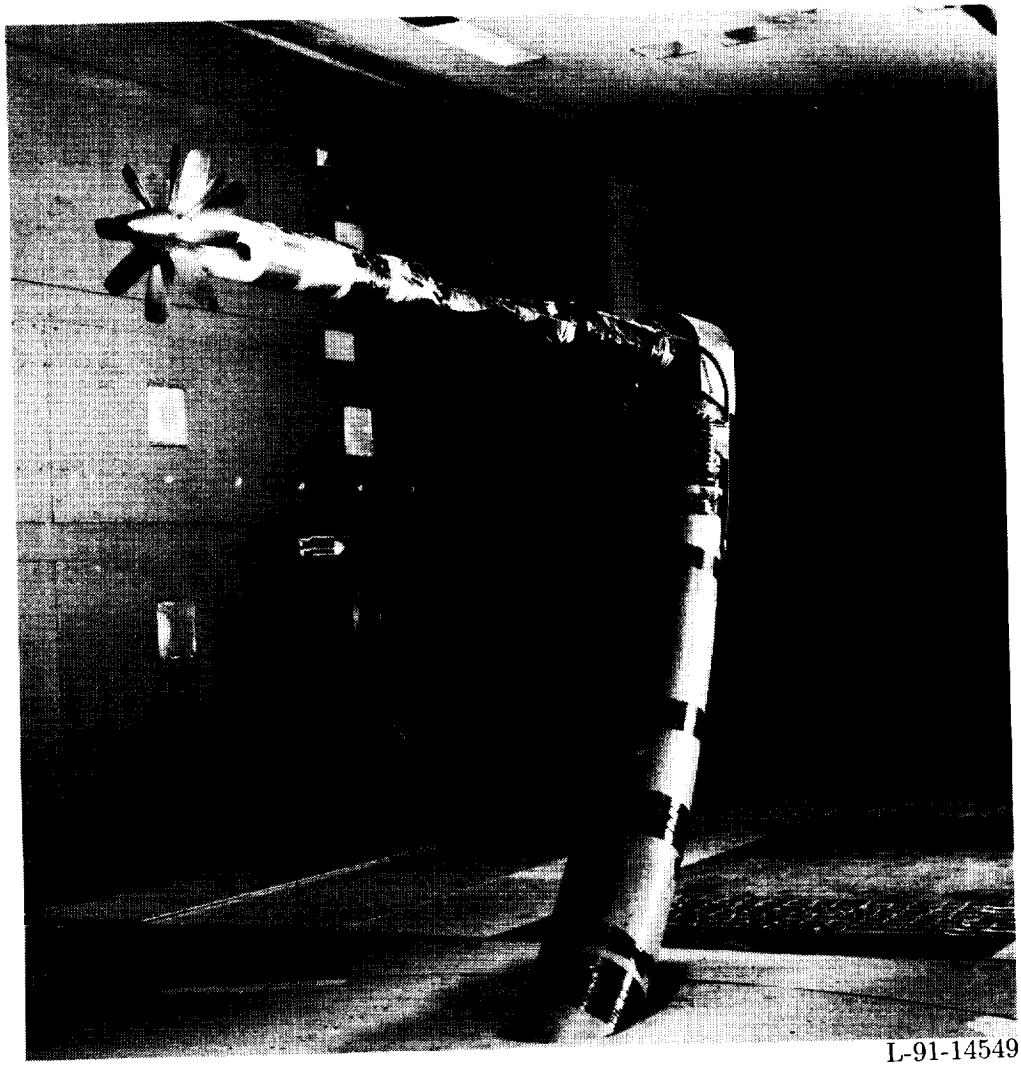

Figure 4. Mounting arrangement of propeller-nacelle model in Langley 14- by 22-Foot Subsonic Tunnel.

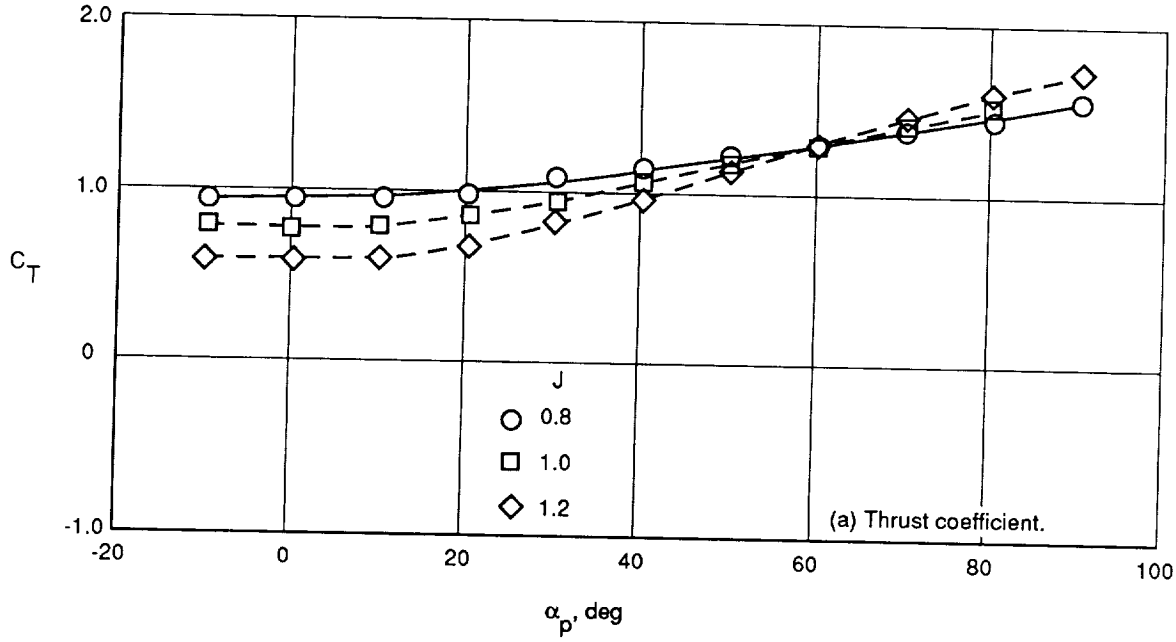

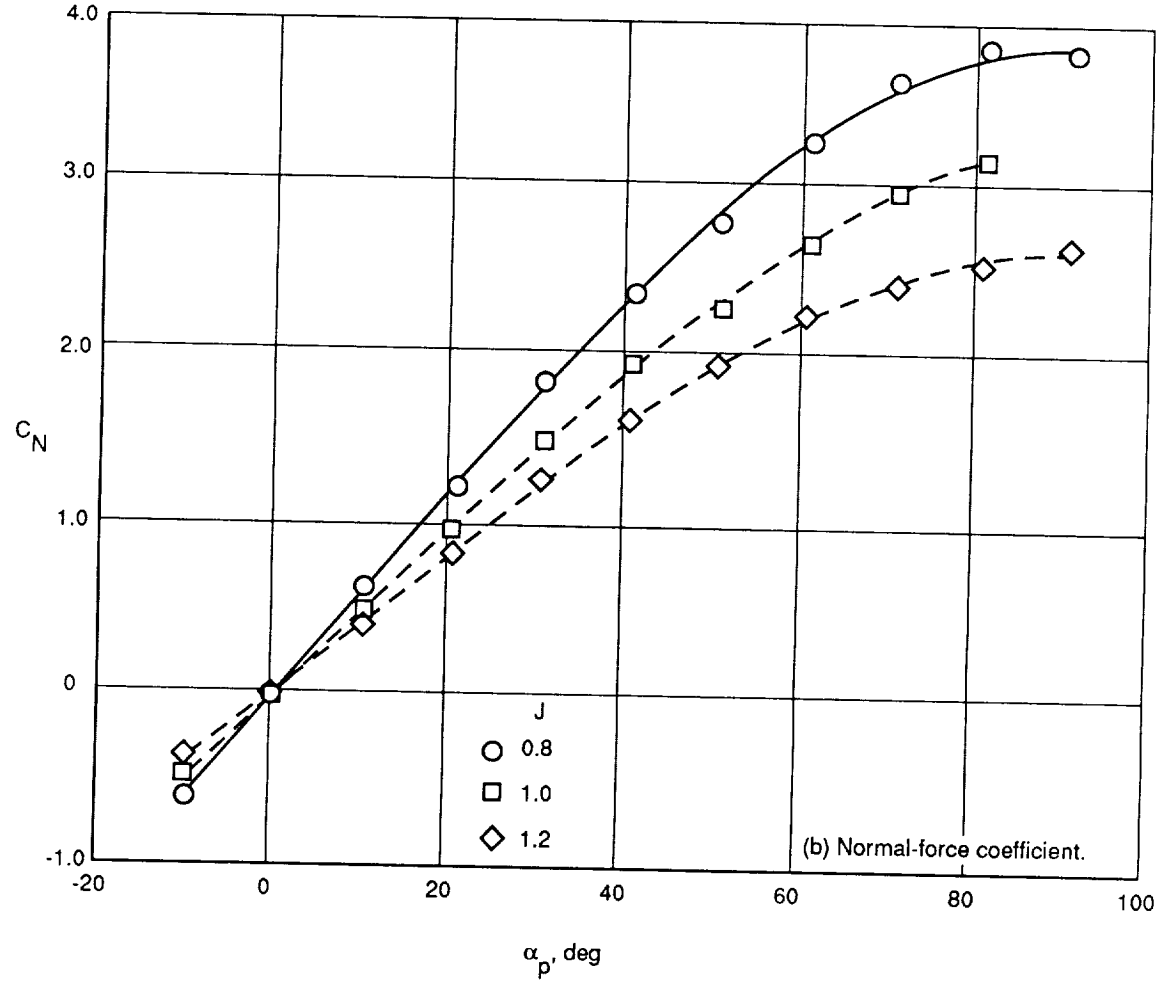

Figure 5. Effect of power on thrust and normal-force coefficients for 8- by 8-blade propeller. $\beta_{0.75} = 36.34°$; $\sigma = 0.56$; $q = 4.5$ psf.

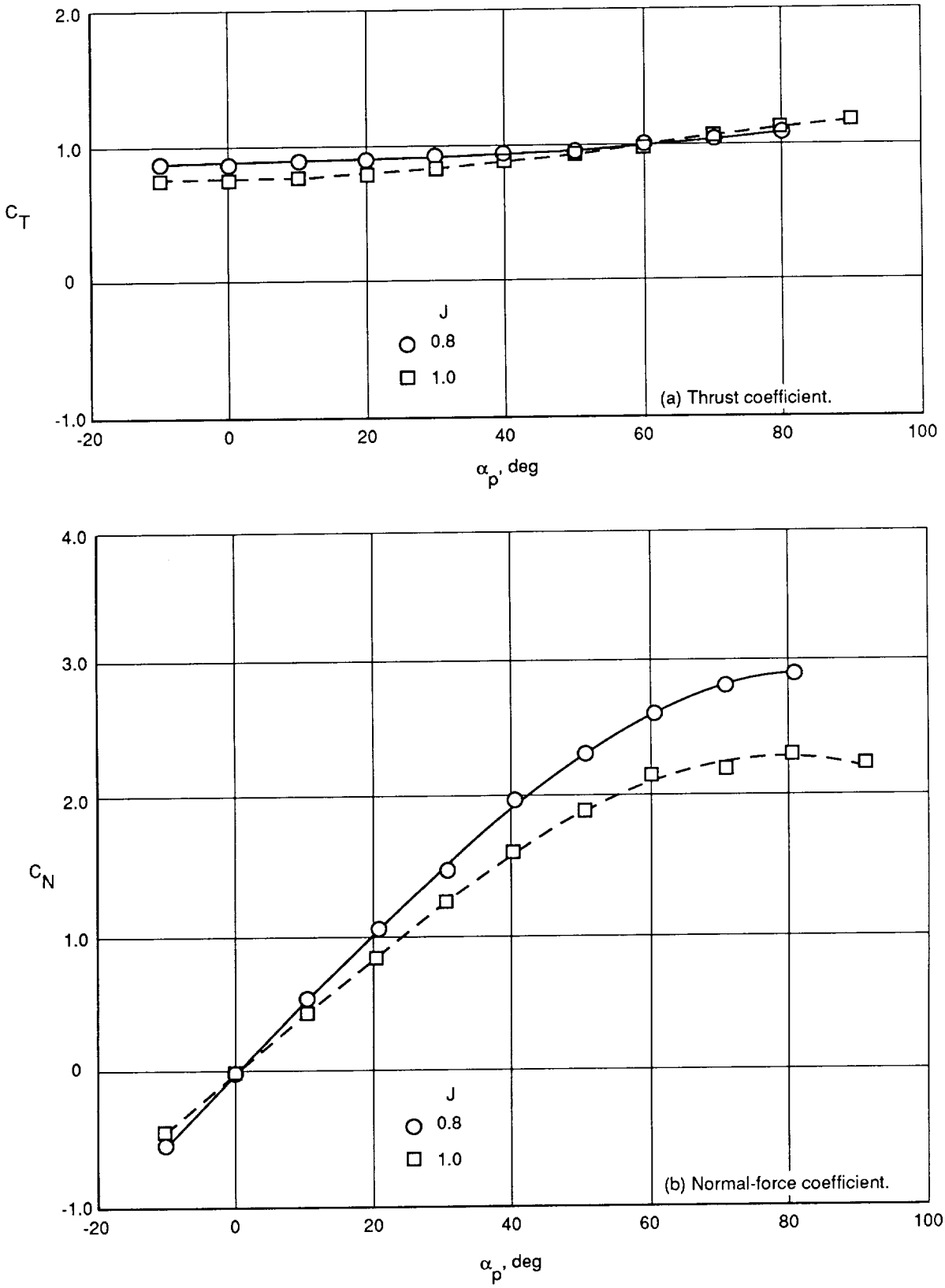

Figure 6. Effect of power on thrust and normal-force coefficients for 4- by 4-blade propeller. $\beta_{0.75} = 36.34°$; $\sigma = 0.28$; and $q = 4.5$ psf.

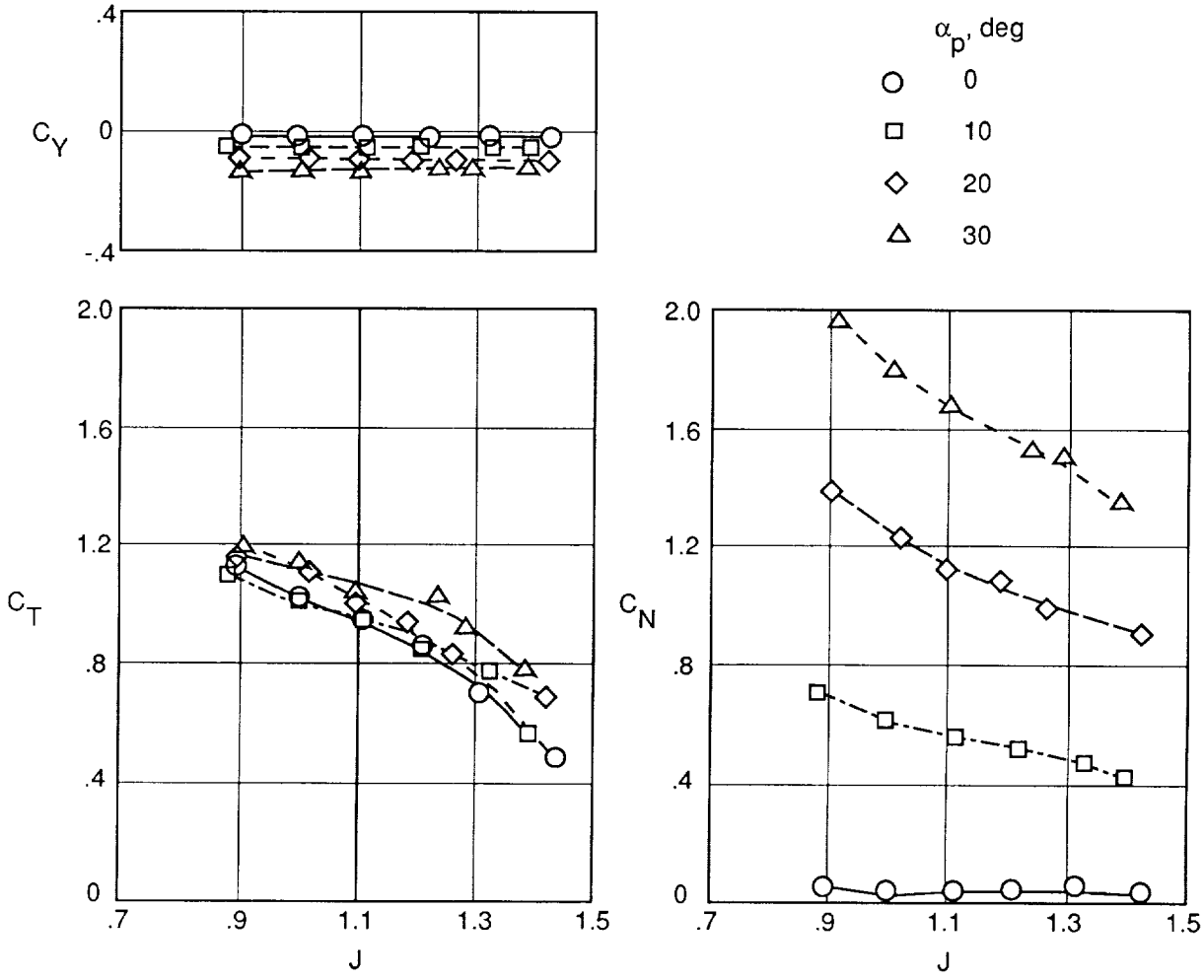

Figure 7. Effect of nacelle angle of attack on propeller thrust coefficient and aerodynamic forces for 8- by 8-blade propeller. $\beta_{0.75} = 41.34°$; $\sigma = 0.56$.

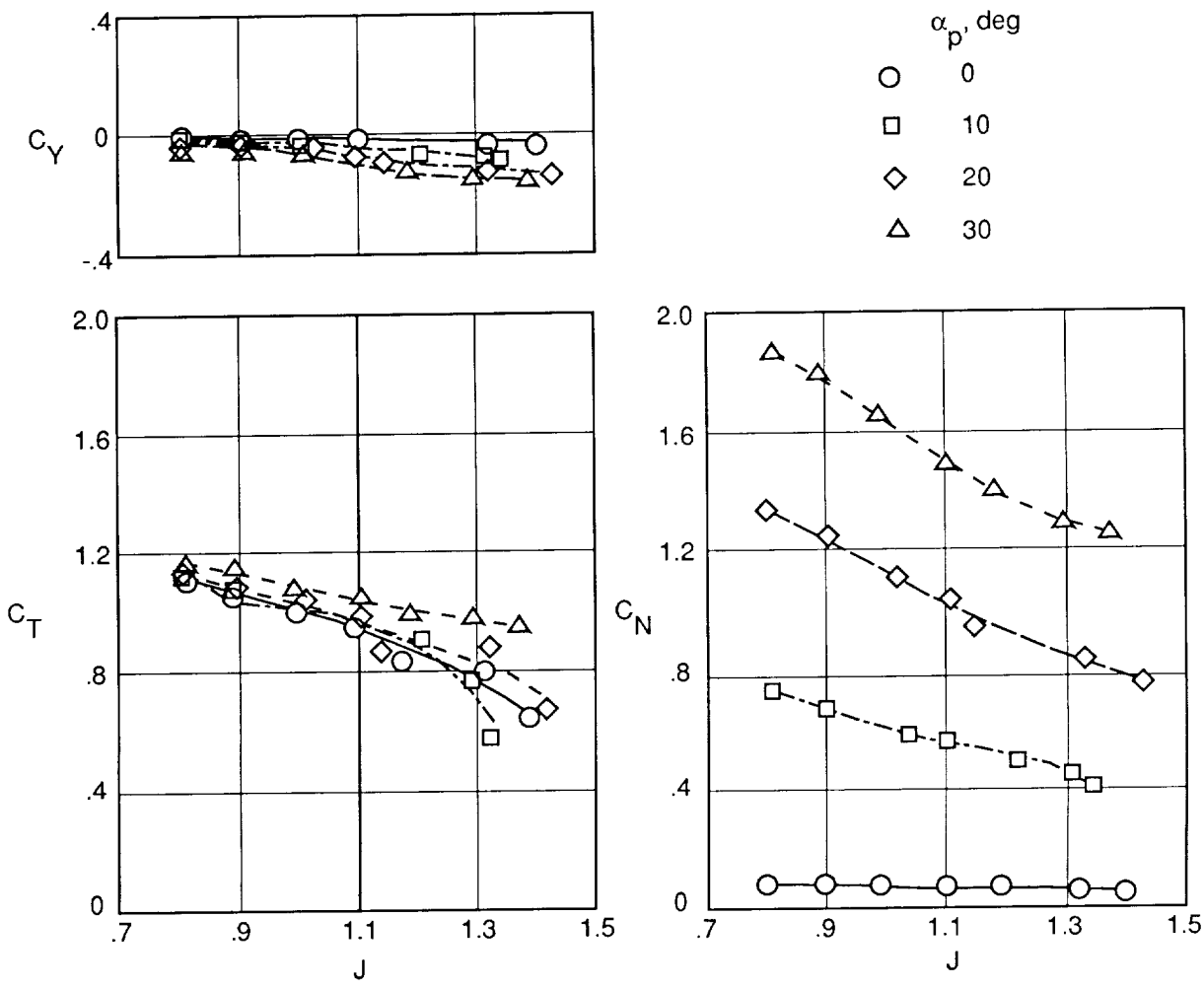

Figure 8. Effect of nacelle angle of attack on propeller thrust coefficient and aerodynamic forces for 8- by 4-blade propeller. $\beta_{0.75} = 41.34°$; $\sigma = 0.42$.

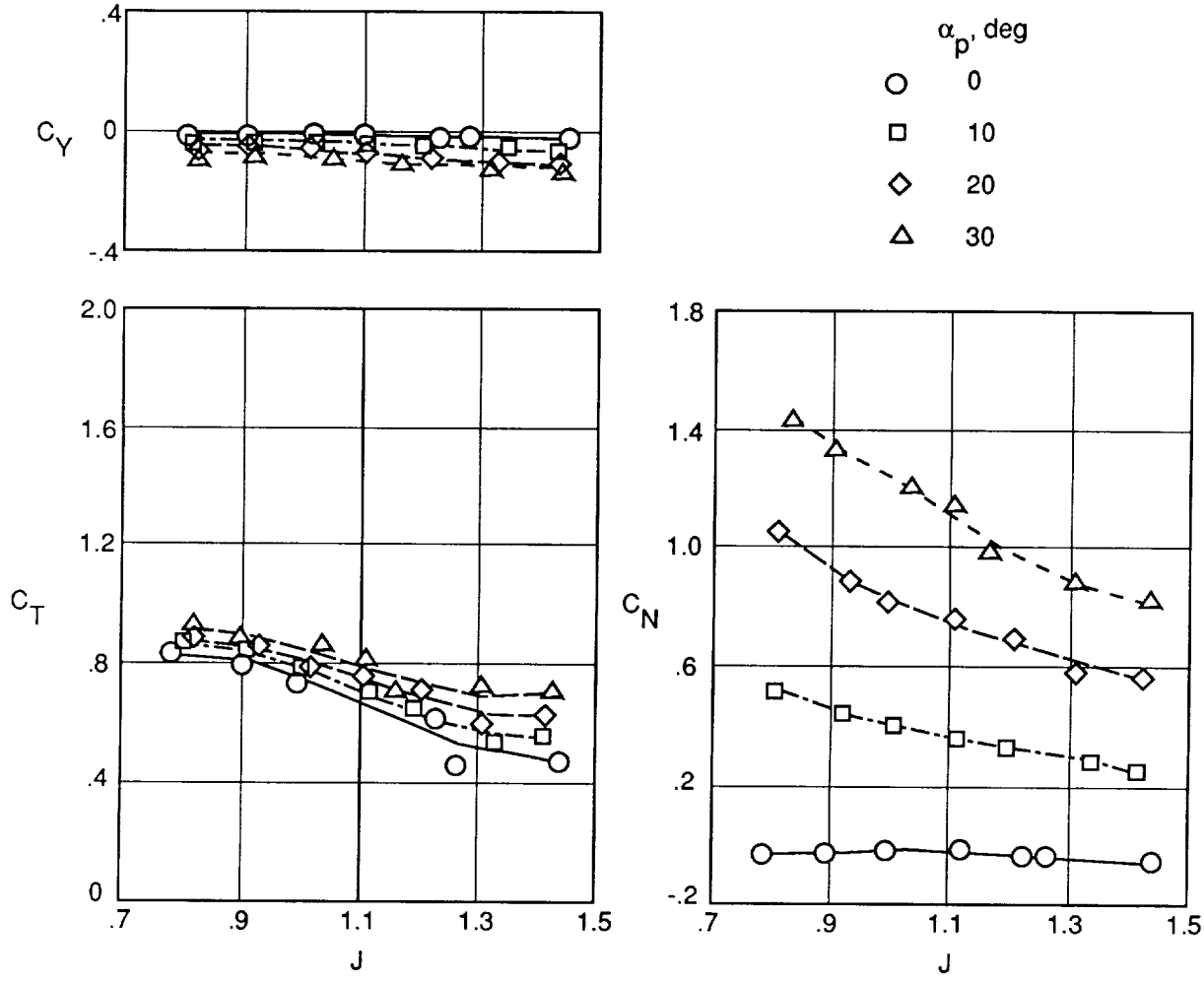

Figure 9. Effect of nacelle angle of attack on propeller thrust coefficient and aerodynamic forces for 4- by 4-blade propeller. $\beta_{0.75} = 41.34°$; $\sigma = 0.28$.

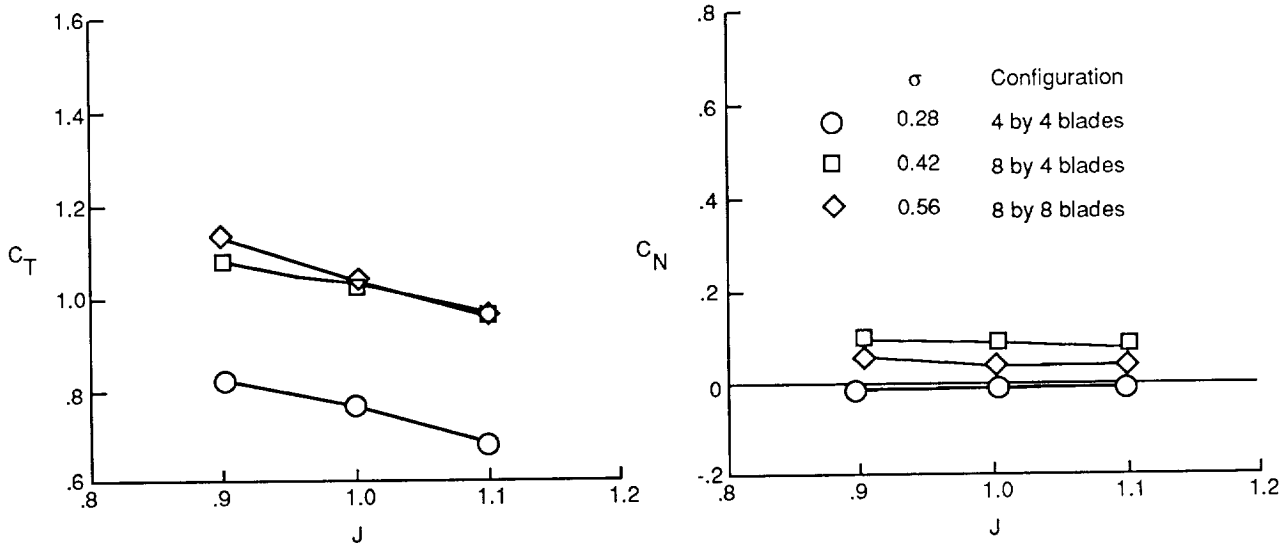

(a) $\alpha = 0°$.

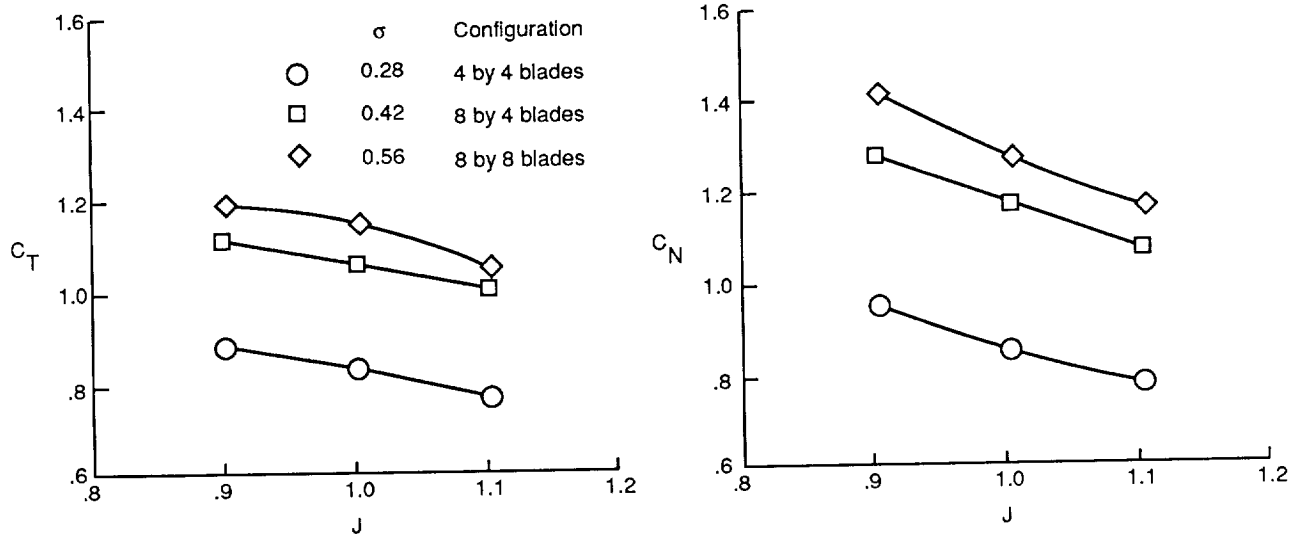

(b) $\alpha = 20°$.

Figure 10. Effect of advance ratio on thrust and normal-force coefficients. $\beta_{0.75} = 41.34°$.

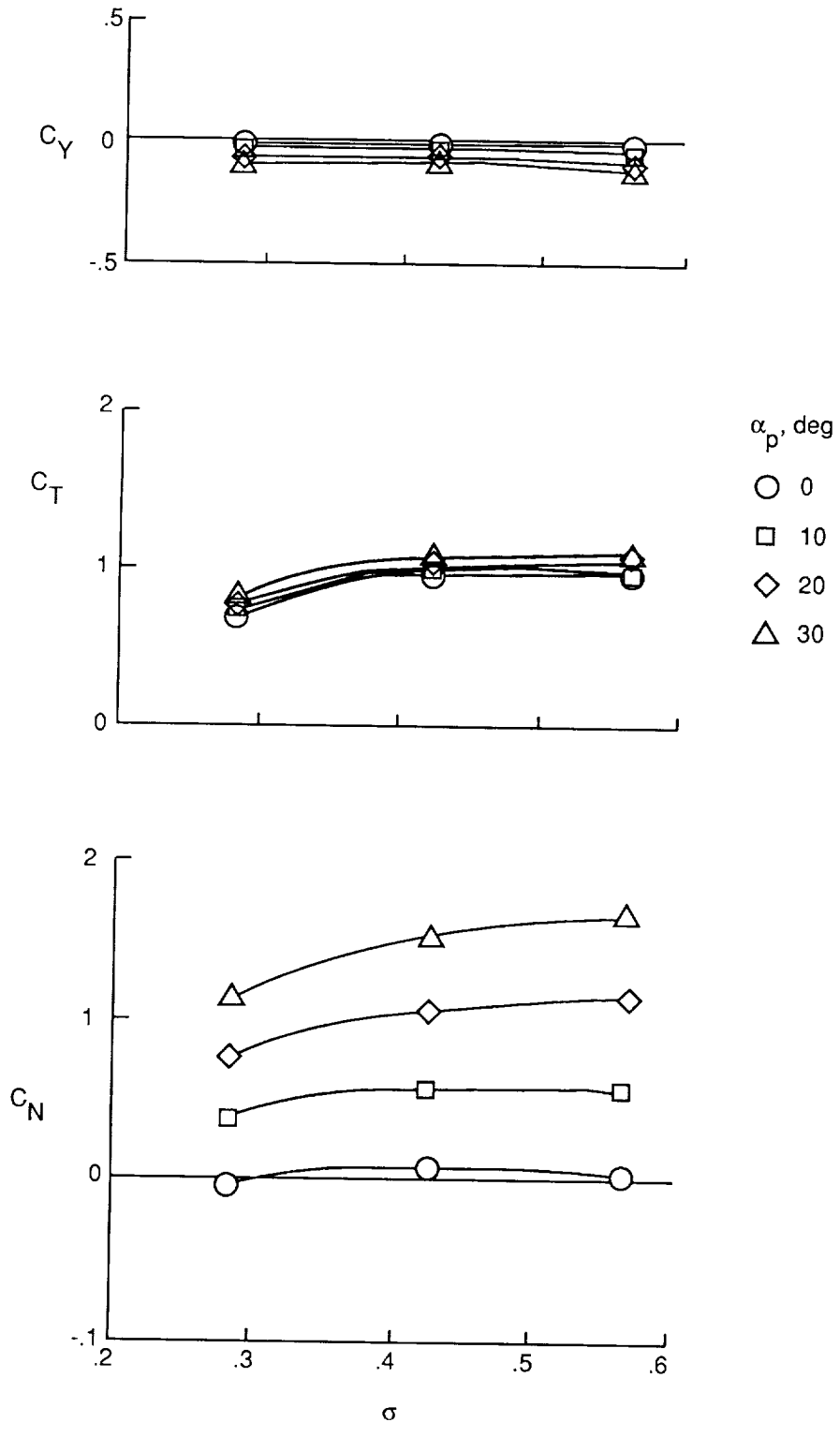

Figure 11. Effect of nacelle angle of attack on side-force, thrust, and normal-force coefficients as function of propeller solidity. $\beta_{0.75} = 41.34°$; $J = 1.1$.

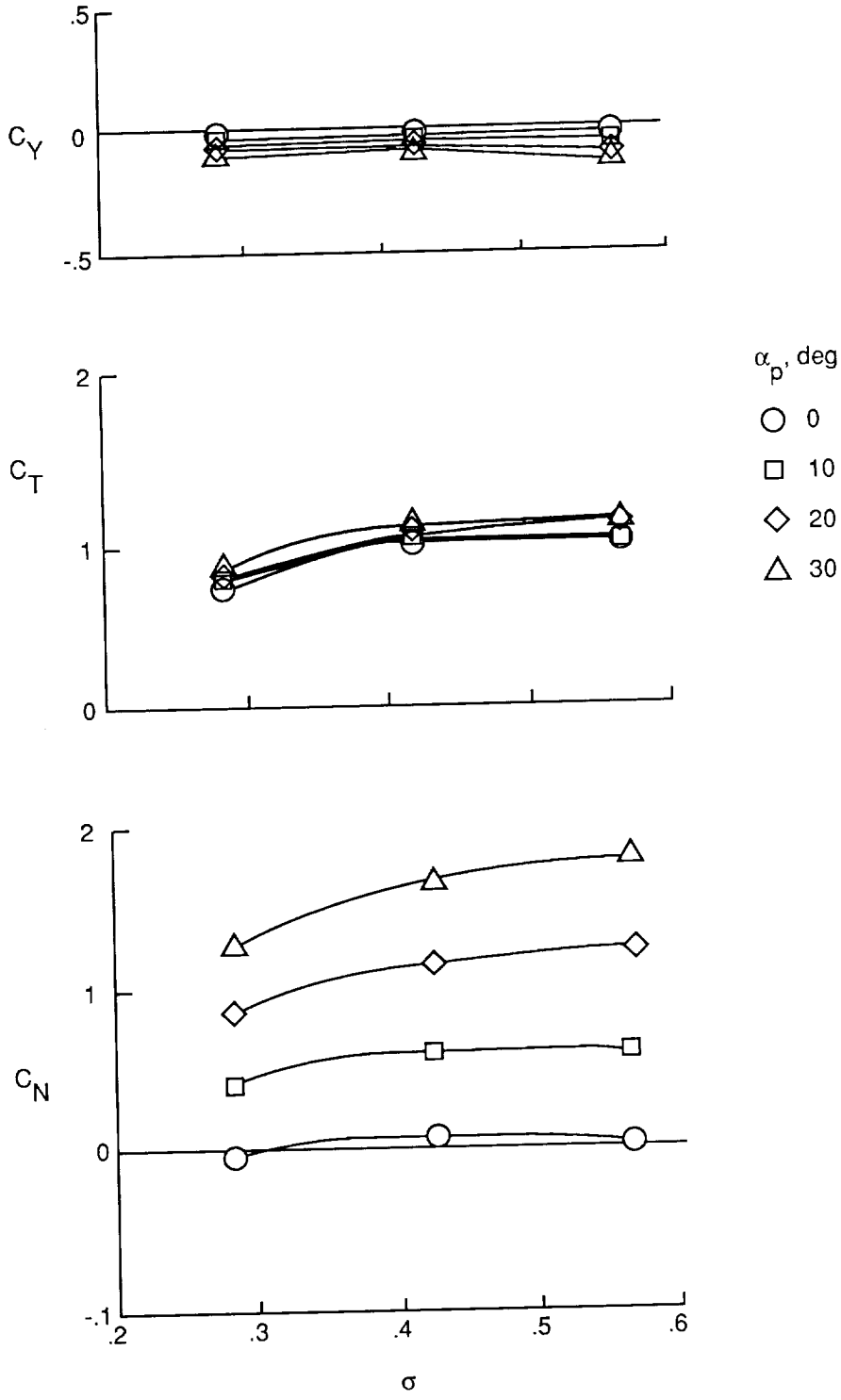

Figure 12. Effect of nacelle angle of attack on side-force, thrust, and normal-force coefficients as function of propeller solidity. $\beta_{0.75} = 41.34°$; $J = 1.0$.

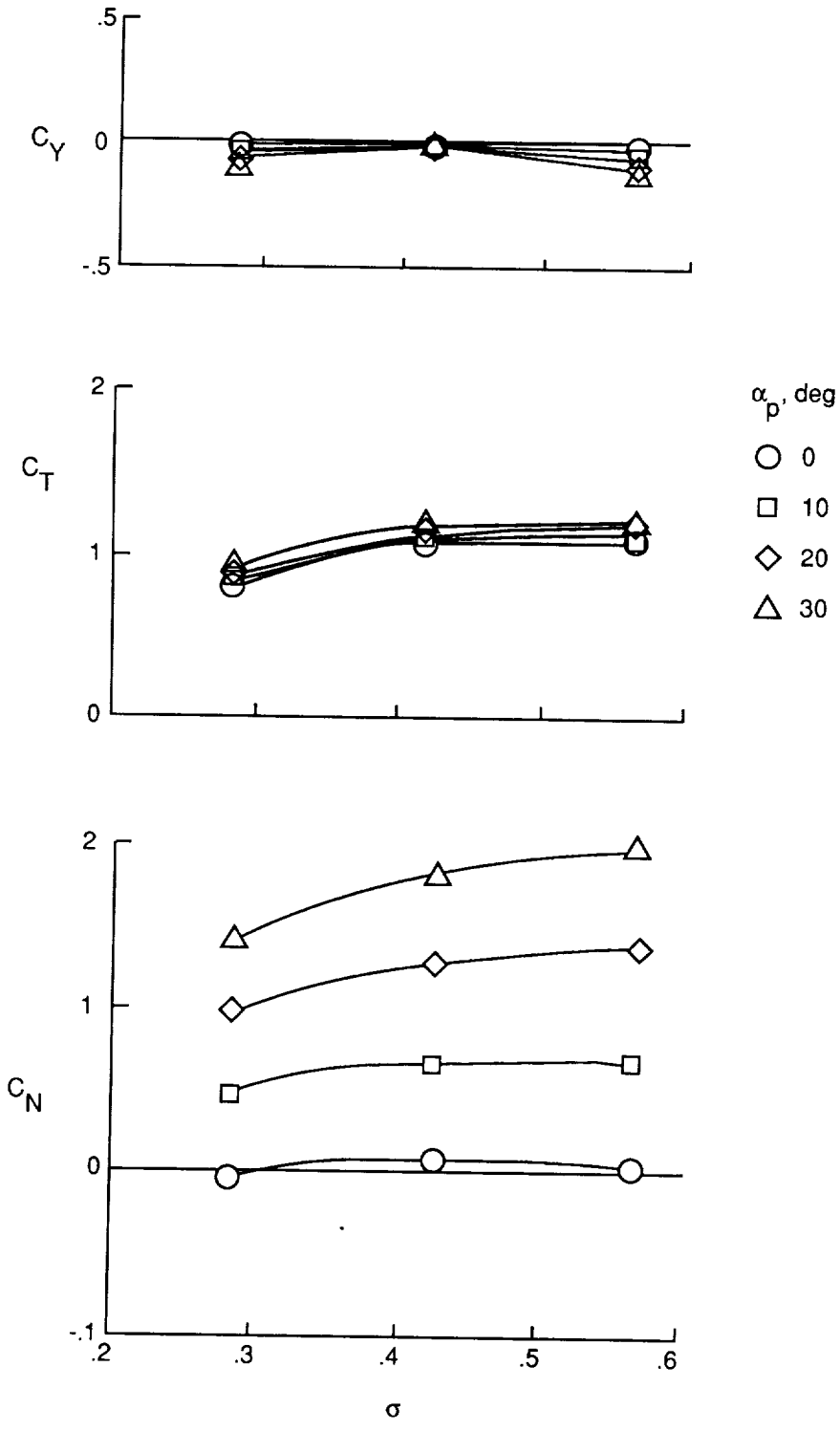

Figure 13. Effect of nacelle angle of attack on side-force, thrust, and normal-force coefficients as function of propeller solidity. $\beta_{0.75} = 41.34°$; $J = 0.9$.

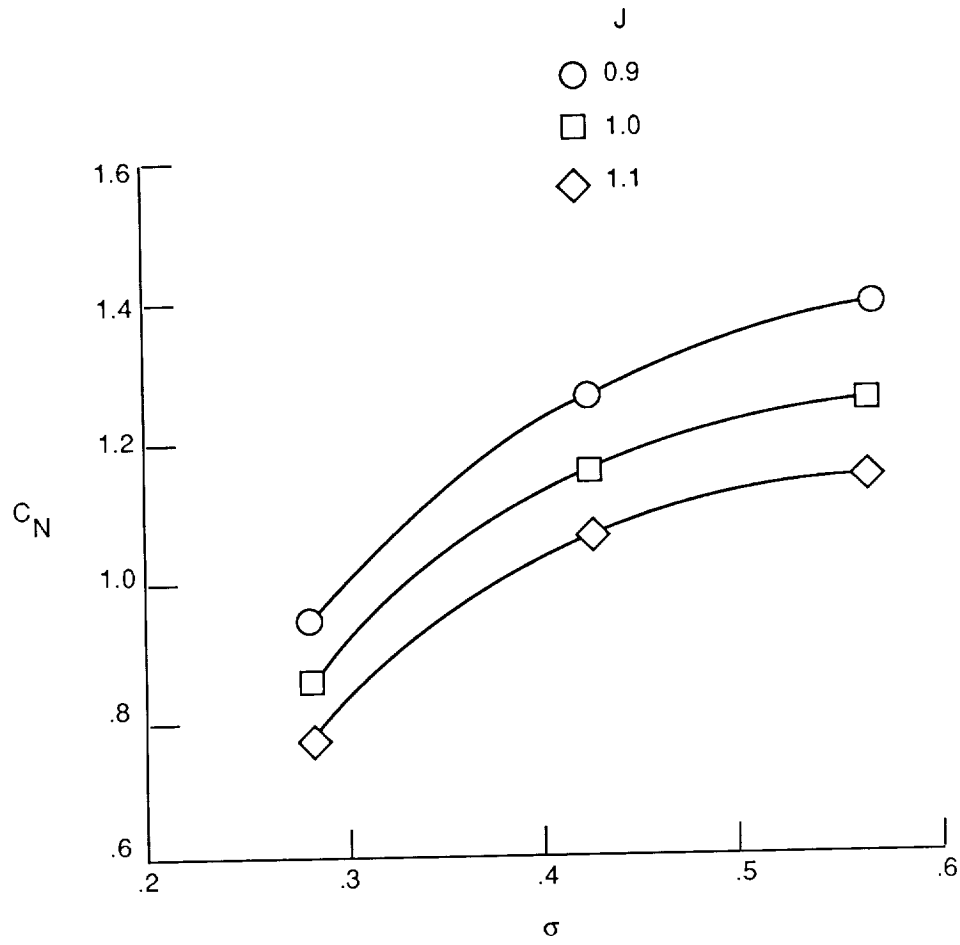

Figure 14. Effect of advance ratio on normal-force coefficient as function of blade solidity. $\beta_{0.75} = 41.34°$; $\alpha_p = 20°$.

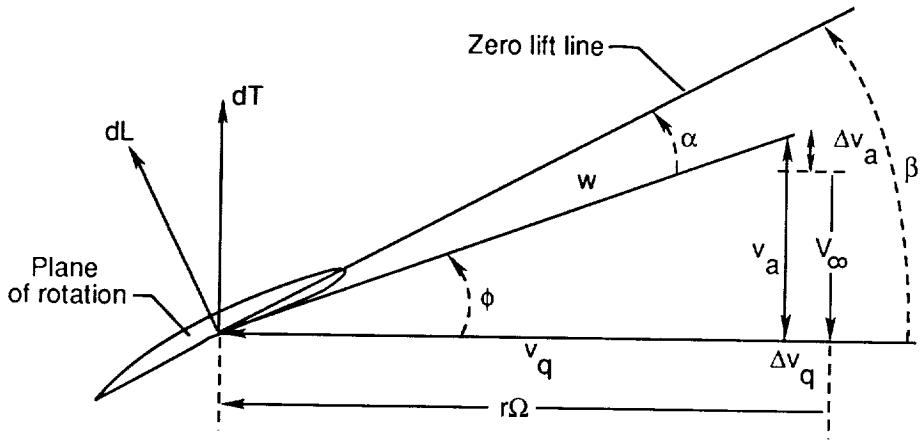

Figure 15. Forces on blade section without propeller inclination.

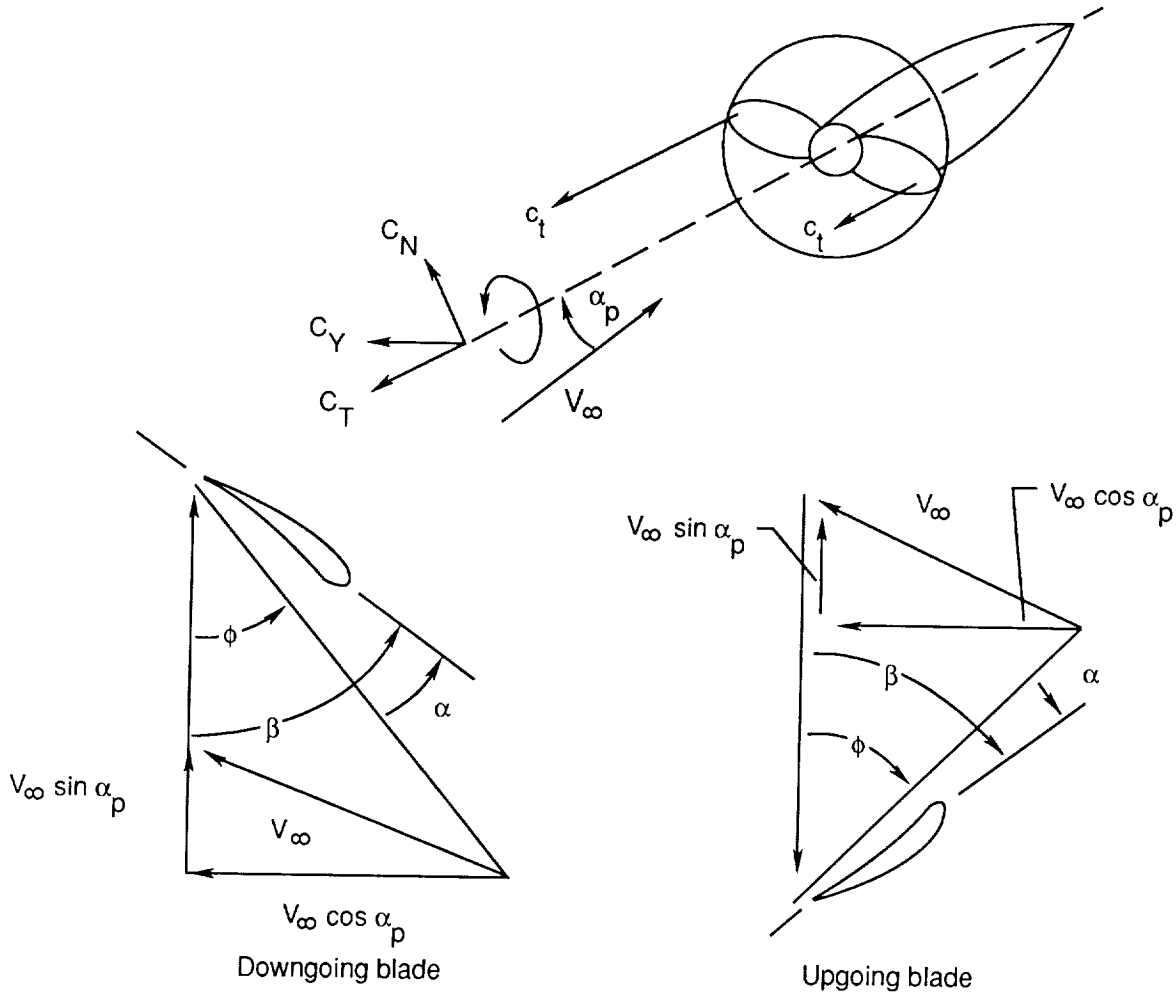

Figure 16. Forces on blade section with propeller inclination.

REPORT DOCUMENTATION PAGE

Form Approved
OMB No. 0704-0188

1. AGENCY USE ONLY *(Leave blank)*	2. REPORT DATE	3. REPORT TYPE AND DATES COVERED
	December 1991	Technical Memorandum

4. TITLE AND SUBTITLE
Effect of Solidity and Inclination on Propeller-Nacelle Force Coefficients

5. FUNDING NUMBERS
WU 535-03-10-02

6. AUTHOR(S)
Garl L. Gentry, Jr., Dana Morris Dunham, and M. A. Takallu

7. PERFORMING ORGANIZATION NAME(S) AND ADDRESS(ES)
NASA Langley Research Center
Hampton, VA 23665-5225

8. PERFORMING ORGANIZATION REPORT NUMBER
L-16933

9. SPONSORING/MONITORING AGENCY NAME(S) AND ADDRESS(ES)
National Aeronautics and Space Administration
Washington, DC 20546-0001

10. SPONSORING/MONITORING AGENCY REPORT NUMBER
NASA TM-4316

11. SUPPLEMENTARY NOTES
Gentry and Dunham: Langley Research Center, Hampton, VA; Takallu: Lockheed Engineering & Sciences Co., Hampton, VA.

12a. DISTRIBUTION/AVAILABILITY STATEMENT
Unclassified Unlimited

Subject Category 02

12b. DISTRIBUTION CODE

13. ABSTRACT *(Maximum 200 words)*
A series of wind tunnel experiments was conducted to study the effect of propeller solidity and thrust axis inclination on the propeller normal-force coefficient. Experiments were conducted in the Langley 14- by 22-Foot Subsonic Tunnel with a sting-mounted, counterrotation, scale-model propeller and nacelle. Configurations had two rows of blades with combinations of 4 and 8 blades per hub. The solidity was varied by changing the number of blades on both rows. Tests were conducted for blade pitch settings of 31.34°, 36.34°, and 41.34° over a range of angle of attack from −10° to 90° and a range of advance ratio from 0.8 to 1.4. The increase in propeller normal force with angle of attack is greater for propellers with higher solidity.

14. SUBJECT TERMS
Turboprop; Counterrotation propellers; Blade solidity; High angle of attack

15. NUMBER OF PAGES
21

16. PRICE CODE
A03

17. SECURITY CLASSIFICATION OF REPORT	18. SECURITY CLASSIFICATION OF THIS PAGE	19. SECURITY CLASSIFICATION OF ABSTRACT	20. LIMITATION OF ABSTRACT
Unclassified	Unclassified		

NSN 7540-01-280-5500

Standard Form 298(Rev. 2-89)
Prescribed by ANSI Std. Z39-18
298-102

NASA-Langley, 1991

National A
Space Ad
Code NIT
Washingto
20546-000